Contact:
cgiganti@lpnhe.in2p3.fr, thorsten.lux@ifae.es

# NP07: ND280 Upgrade project
# -
# SPSC Report

*The T2K ND280 Upgrade Working Group*

**Abstract**

The upgrade of the T2K Near Detector, ND280, has been approved by the SPSC in April 2019 and it is one of the Neutrino Platform projects (NP07). In this document, prepared for the SPSC Annual review, we summarize the main milestones obtained in the last year of the project towards the installation of the detectors at J-PARC expected to be completed by the end of the calendar year 2023.

CERN-SPSC-2023-015 / SPSC-SR-328
02/05/2023

Version 1.0
May 2, 2023

# 1 T2K and the ND280 upgrade project

The T2K experiment is a long-baseline neutrino oscillation experiment, currently ongoing in Japan. T2K has been the first experiment to detect the appearance of electron neutrinos in a muon neutrino beam and is now searching for CP violation in the leptonic sector by precisely measuring appearance probabilities of neutrino and antineutrinos. Such measurement requires both, larger statistics and a better understanding of systematic uncertainties. In order to improve both, an upgrade of the T2K Near Detector, ND280, is being conducted and is expected to significantly reduce the impact of systematic uncertainties on T2K oscillation analyses and, more in general, to improve the current knowledge of neutrino cross-section models.

The ND280 upgrade, shown in Fig. 1, will consist in replacing one of the sub-detectors, the P0D, the most upstream inner detector of ND280, with two horizontal TPCs (HA-TPC) and a horizontal fully active carbon target in the middle (Super-FGD). Six Time-of-Flight (ToF) planes will be installed around the HA-TPCs and the Super-FGD.

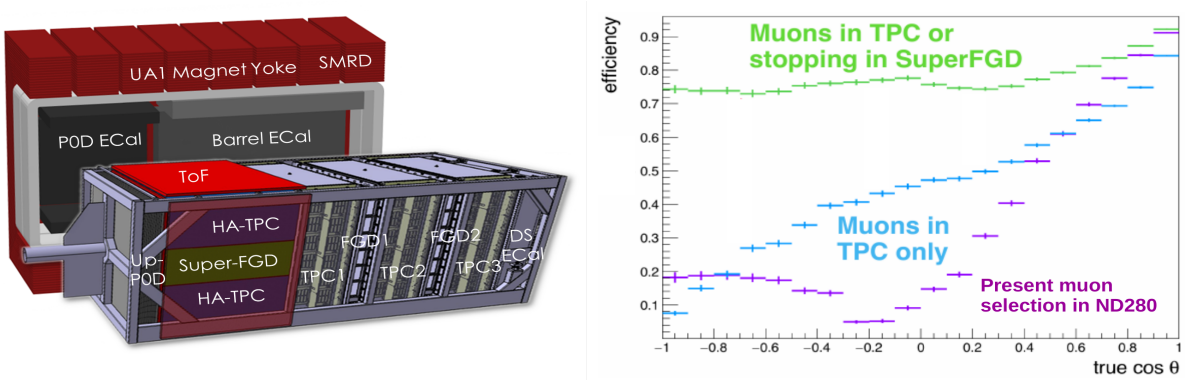


Figure 1: Left: Sketch of the ND280 upgrade project, including Super-FGD (green), HA-TPC (violet) and ToF modules (red). Right: ND280 upgrade efficiency in reconstructing muons (right) .

The main improvements that will be obtained thanks to the upgrade with respect to the current Near Detector configuration are:

- higher efficiency in reconstructing muons produced in neutrino interactions and emitted at high polar angle with respect to the neutrino direction, thanks to the two high angle TPCs. (see Fig. 1 right)
- higher efficiency in detecting low momentum protons and pions produced in neutrino interactions thanks to the high granularity and the 3D reconstruction capabilities of the Super-FGD .
- the ability to more reliably tag neutrons, and to measure their momenta using thier time of flight from the neutrino interaction vertex thanks to the excellent position and timing resolution of the Super-FGD.

In this document we focus on the project progress since the last SPSC review in April 2022. For further details, we refer to two recent publications [1, 2] as well the TDR describing the ND280 upgrade [3] which was finished in 2019 and was the basis for being approved as Neutrino Platform project NP07 by the SPSC in April 2019. The MoU between CERN and all participant institutes have been signed in summer 2020. In addition, a list of recent papers in which more details about NP-07 can be found is given here:

- Study of final state interactions of protons in neutrino-nucleus scattering with INCL and NuWro cascade models [4];
- Analysis of test beam data for ERAM detectors [5, 6]

- Characterization of ERAM detectors with the test bench at CERN [7]
- Super-FGD prototype time resolution [8]
- Total neutron cross-section measurement on CH with a novel 3D-projection scintillator detector [9]
- Use of artificial intelligence for Super-FGD reconstruction [10]

The current status of the detectors is as follow: all the components for the Super-FGD, with the exception of the electronics, are already in Japan and have been assembled at J-PARC. This includes the installation of the cubes into the box, the replacement of the fishing lines with the optical fibers, and the installation of the MPPC boards. Green light for the production of the Super-FGD electronics has also been recently given and the production is on-going. We expect to ship the electronics to J-PARC in July 2023.

For the High-Angle TPCs, a serious electrical problem was found affecting the first HA-TPC field cage. Understanding this issue required a huge campaign of tests and measurements that were done at CERN in Spring and Summer 2022. Minor modifications to the production of the Field Cage were put in place before restarting the production and the first newly produced field cage was received at CERN in February 2023 and extensively and succesfully tested in the last two months. The second half of the field cage, needed to complete the bottom TPC, is expected to be received at CERN in May 2023.

Concerning the Time-Of-Flight detector, the six planes have been assembled and tested at CERN and are ready to be shipped to J-PARC.

## 2 The Super-FGD

The Super-FGD [11] is a novel design of fine-grained fully-active plastic scintillator detector (Fig. 2). It consists of about two million optically-independent $1\times1\times1$ cm$^3$ cubes of plastic scintillator, read out along the three orthogonal directions by wavelength shifting (WLS) fibers, each one coupled at one end with a Multi-Pixel Photon Counter (MPPC). The active part consists of $192\times182\times56$ cubes. The total weight of the Super-FGD is about 2 tons, doubling the target mass and thus statistics compared to the existing ND280 tracker detector. At the same time, the reconstruction efficiency for particles with angles larger than approximately $60^\circ$ with respect to the neutrino beam direction is ensured with high accuracy and low systematic uncertainties as well as down to lower momentum threshold. Hence, the main limitation of the existing ND280 detectors will be overcome. Moreover, such detector will give us the opportunity to reconstruct the kinematics of neutrons present in the neutrino interaction final state, thanks to the time-of-flight (tof) technique.

In this section, we report about the progress of the detector production, assembly and the preparation for the upcoming commissioning. The final results of the neutron beam tests at the Los Alamos National Laboratory using Super-FGD prototypes are also reported.

### 2.1 Progress on detector production and assembly and plans for commissioning

Fifty-six layers of $192 \times 182$ cubes were assembled at INR Moscow before the end of 2021, and delivered to J-PARC in June 2022. A platform consisting of a support and a top access system was designed and produced at JINR Dubna in 2021 for the cube and mechanical box assembly and was delivered to J-PARC in July 2022. The production and machining of the six plates of the Super-FGD carbon and glass fiber based mechanical box was slowed down by issues related to Covid19 but completed in Summer 2022. Box assembly and loading tests were successfully performed at CERN in August and September 2022: the box was fully assembled, mounted and held at the four corners on a mechanical frame to reproduce the ND280 detector configuration and filled with approximately 3.5 tons of sand bags. The maximal sagging on the bottom panel was less than 3 mm and consistent with the design specs. Eventually, the six box plates were dismounted and delivered on the 24th of October to J-PARC

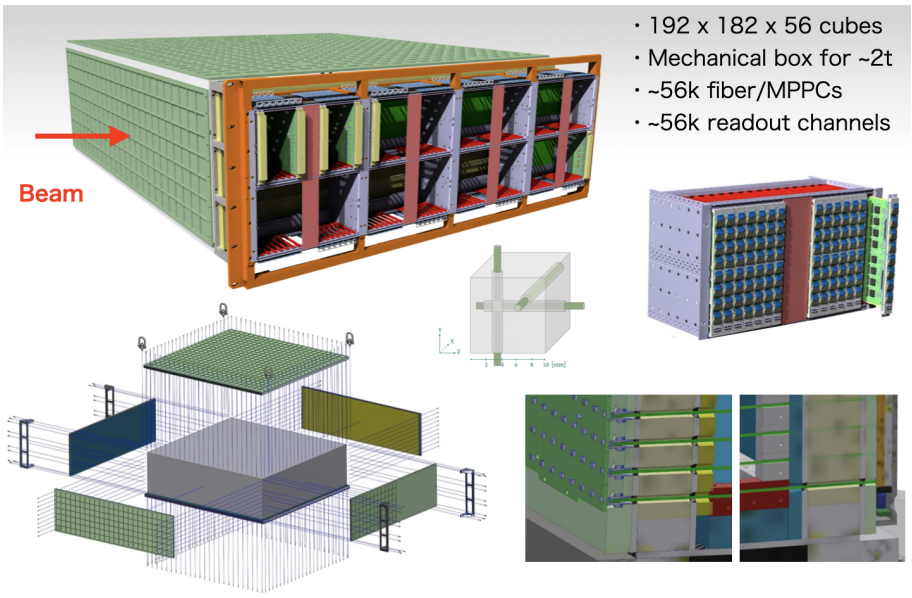


Figure 2: Detector design of the Super-FGD.

where, soon after, the detector assembly started. Figure 3 shows photos of the major steps in the detector assembly: (i) we started with the assembly of the support system and top access systems; (ii) after three box panels were installed on the support system, the assembly of the cube layers in the box could start; (iii) it took 18 working days to assemble all the 56 layers. We carefully aligned the cubes with about 112'000 box holes using dedicated tools (reference aluminum cubes and spokes, long metallic rods and surveying equipment); (iv) in order to close the box, wooden panels used to hold the cubes in the right position were removed; (v) the two side box plates were closed after threading the fishing lines through all the holes. In total, approximately 13'000 long rods were used to keep the cube vertical alignment and easy the closure of the top panel.

The second part of the detector assembly was performed after modifying the configuration to provide the same mechanical boundary conditions as the final ones in the ND280 basket: (vi) we transferred the detector into a new mechanical support and fixed by aluminum brackets at the four corners, to fake the ND280 basket configuration. The measured sag at the center was about 3 mm, consistent with the FEA results and design specs; (vii) we replaced the fishing lines with WLS fibers, starting from the horizontal longer ones to mitigate the risk of cube hole misalignment. It took about 10 working days by 10 workers $\times$ 2 shifts per day for about 21'000 long fibers. Quality checks of all fibers were performed soon after the assembly using a dedicated setup with array of high-intensity LEDs and photo-sensors; (viii) then the PCBs with sixty-four surface-mounted MPPCs (MPPC64-PCB) were mounted, being guided by a developed mapping database on GUI; (ix) the shorter vertical fibers were assembled in the same way, though by replacing metal rods with fibers. It took about 10 working days by 8 workers $\times$ 2 shifts per day for 35'000 short fibers; (x) in the same way, the top MPPC64-PCBs were assembled after the quality check.

The Super-FGD is equipped with the LED calibration system injecting light at the WLS fiber end not coupled with an MPPC. Therefore, we had to cut all the WLS fibers at the very end of detector plates before ensuring the detector light tightness: (xi) after the fiber cutting work, 46 and 47 optical modules for the LED calibration system were attached to the box bottom and side panels, opposite to those instrumented with MPPC64-PCBs; (xii) the entire detector external surface was covered by light barrier sheets so that Super-FGD can work in a totally-dark environment. A total of 881 cables were attached to the MPPC64-PCB connectors after passing them through a thin slit in the light barrier. In order to further enhance the detector light tightness, black tape and silicone were also used. Connectivity and light tightness were confirmed with tests using a commercial CAEN DT5702 read out electronic boards

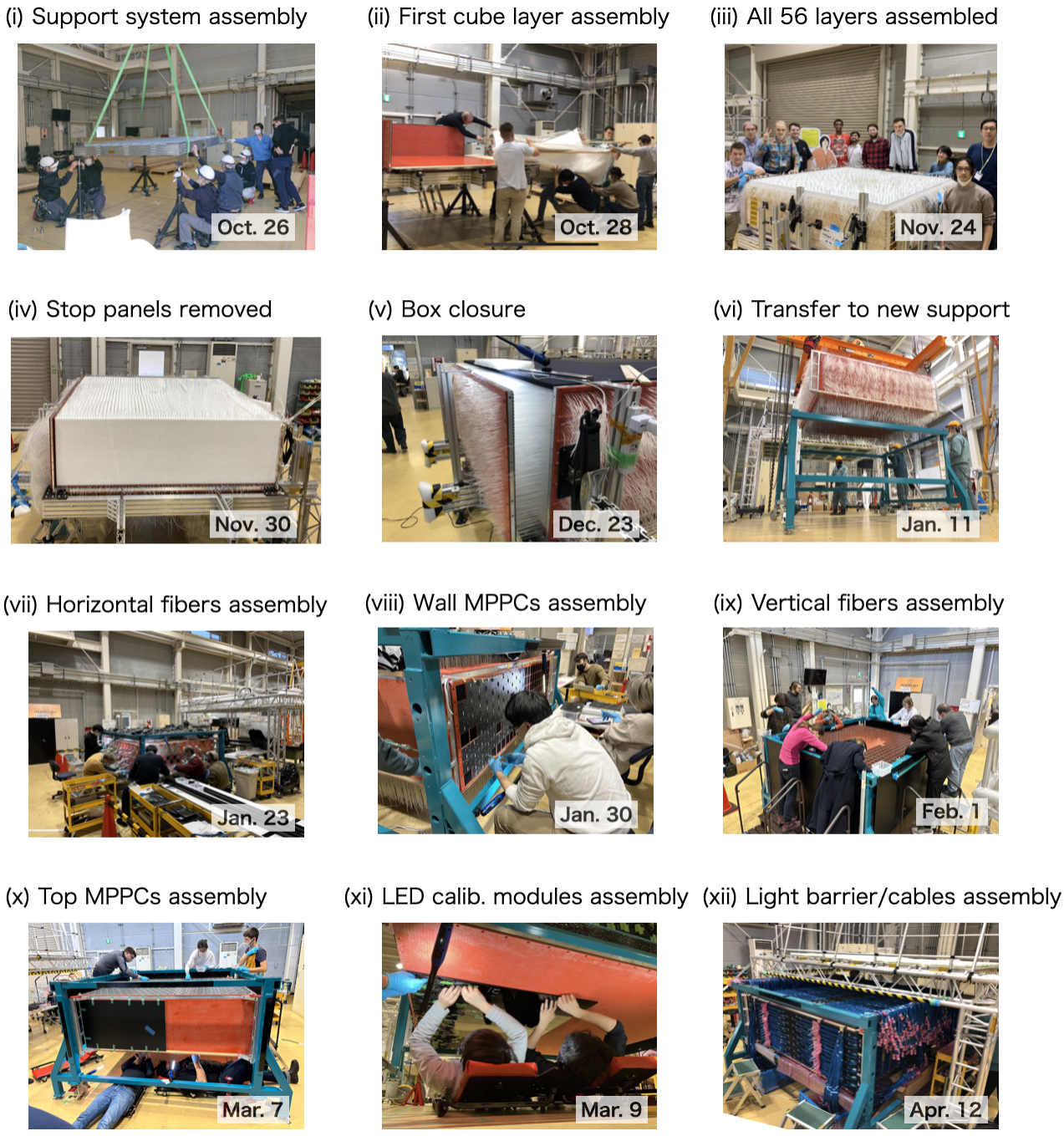


Figure 3: Detector assembly at J-PARC.

(design based on the CITIROC ASIC, the same as used in Super-FGD). The problematic channels were identified and fixed. No dead channels have been found so far. As a bonus from the tests, we successfully obtained single photoelectron (PE) distributions from LED runs as well as cosmic events, both shown in Fig. 4.

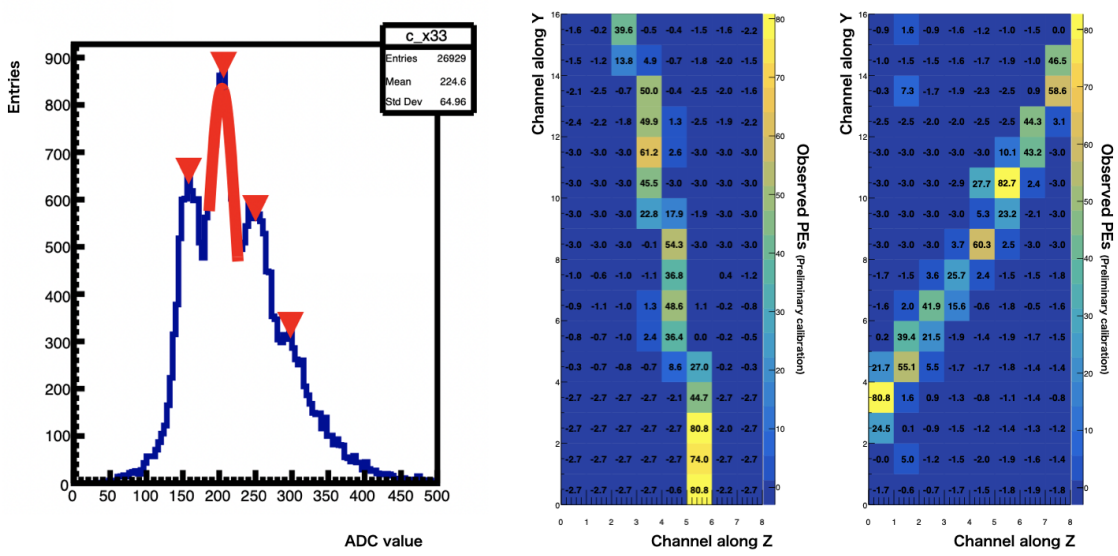


Figure 4: Left: ADC distribution with single PE resolution for a channel obtained with an LED run. Middle and Right: two cosmic events detected with two consecutive MPPC64-PCBs read out with CAEN DT5702 electronic board.

Meanwhile, the Super-FGD electronics project has also advanced. The design of the electronics has been completed and validated with prototypes and the mass production has started. The production and assembly of the Front-End Boards (FEB) is taking place in Europe and is expected to be completed in early July. We expect to complete the fabrication in U.S. of the Back-End Electronics (optical concentrator boards, master clock board and back-plane) around the middle of June. The overall electronics integration with relative quality checks will be performed at the University of Geneva between June and July and sent to J-PARC in different batches.

The preparation for the on-surface commissioning has started in J-PARC in April using a vertical slice test bench, already used in Europe and US to validate the prototypes in order to provide the green light for the mass production of the electronics components. Our plan, until the electronics delivery to J-PARC, is to prepare for data taking and processing using the real detector and the vertical slice test bench toward smooth transition to a regular detector operation. We then expect it will be possible to confirm the readiness of the detector soon after the full electronics installation.

Such preparation includes the overall validation of the DAQ and Slow Control systems, the completion of the data unpacking software and related integration in the full data analysis software chain. At the same time, the calibration methods and related software developments are ongoing in coordination with the physics working groups.

The full on-surface commissioning will take place exactly where Super-FGD has been assembled and will start when the first electronics batch will arrive in J-PARC around the middle of July. It will continue over August with both LED and cosmic runs to verify the cable mapping, connectivity, etc. until the functioning of the full detector has been confirmed. We expect to start the Super-FGD installation in the ND280 basket in early September and collect about twenty more days of cosmic data to perform the final checks to be ready for the first neutrino beam run.

### 2.2 LANL neutron beam test results

The characterization of the Super-FGD response to fast neutrons is crucial for the successful detection of neutrons produced by neutrino and anti-neutrino interactions and the consequent reconstruction of their kinematics with the tof technique. The so-called Super-FGD and the US-Japan prototypes have been exposed to neutrons with energies between 0 and 800 MeV at the Los Alamos National Laboratory (LANL) Weapon Nuclear Research (WNR) facility in December 2019 and 2020. The neutron tof was measured with a resolution of 1.37 ns.

The measurement of the total neutron-CH cross section has been completed and is shown in Fig. 5. The details of the data analysis including the full study of the systematic uncertainties have been published in Physics Letters B [12]. Such result, consistent with existing data, is a powerful demonstration of our solid understanding of the detector response to neutrons in view of the first-ever reconstruction of the neutron kinematics in final-state neutrino interactions.

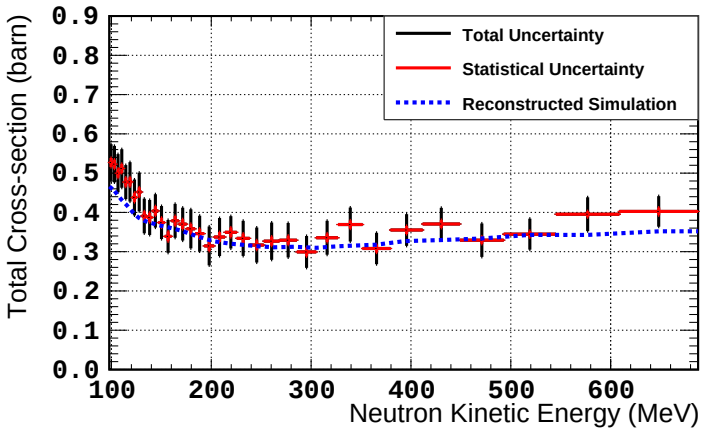


Figure 5: Total neutron-CH cross-section as a function of the neutron kinetic energy is shown together with the total (black error bars) and the statistical (red error bars) uncertainties. The simulated total cross section obtained with the Geant4 `Bertini` model is shown by the blue dashed line. Figures are taken from [12].

## 3 The High-Angle TPCs

### 3.1 Status of the Field Cages

The HATPC is made up of two Field Cages joined at the central cathode plane. Each Field Cage is 175 x 84 cm² in size with a drift length of 99 cm. The device is readout by 16 Encapsulated Resistive Anode bulk Micromegas modules at the two opposite Anodes, which cover the entire transverse surface.

The Field Cage structures are produced by the NEXUS Company in Barcelona using composite material techniques on an Aluminum mold from INFN. The inner surface is covered by the field shaping electrodes, consisting of two layers of copper strips that are interleaved and partially overlap to minimize electric field non-uniformities. The Field Cage structures are made extremely stiff by two layers of 2mm thick aramid fabric interspaced by 3.5cm aramid honeycomb.

Due to a serious electrical issue with the first full scale Field Cage (FC0) caused by contaminated insulating layers within the Cage structure, the Cages production was stopped from April 2022 to October 2022, until we completely understood and solved the issue. The second Field Cage (FC1) was delivered to CERN in late February 2023 and was successfully qualified in terms of mechanical, electrical, and gas quality. FC1 has been set up with a special cathode endcap and 8 ERAM modules

to be read out as the first "half" HATPC, which will be qualified with Cosmic Rays at CERN bld 182. The production of the third Field Cage is well advanced and is expected to be delivered in early May, so that the assembly of the first HATPC can be completed by the end of June.

In the paragraphs that follow, we will summarize the electrical issue that occurred with FC0, the solution that was implemented to address it, the characterization of FC1 in terms of its mechanical, electrical, and gas quality, and the preparation for the assembly of the first HATPC in Bld 182 at CERN.

### 3.1.1 THE HIGH VOLTAGE ISSUE WITH THE FIRST FIELD CAGE (FC0)

In early March 2022, the NEXUS company delivered the first full-scale Field Cage (FC0) to CERN. It passed metrology validation and mechanical tests, including tests for gas tightness. We began electrical testing in early April 2022. When we applied a negative voltage ("HV") to the Cathode (K), we measured an excessive divider current, exceeding what we expected based on the HV/Rd ratio (Rd being the full resistance of the voltage divider). This indicated the presence of alternative current paths from the Anode to the Cathode, running parallel to the resistive divider. The extra current was approximately $5A$ at an HV of $-10kV$ ($I_{ex}/I_{divider} \sim 50\%$) and increased non-linearly with the voltage. We observed that as soon as HV was applied, the extra current spiked at high values (several $A$) and slowly decreased over time. After several minutes, it reached a constant asymptotic value with a time constant that depended on the applied voltage HV. This suggests that the effect was due to either electrical parts with large RC values or dielectric relaxation phenomena (or both). We did not observe any such extra current effects at any level when operating a small-scale Field Cage prototype built using the same processes. The only difference was the transverse dimensions of the inner volume, which were 42x42 $cm^2$ instead of 175x84 $cm^2$, resulting in an inner surface area that was smaller by a factor of 3 compared to the full-scale HATPC Field Cage.

**Cause of the High Voltage issue in Field Cage Production**

After several careful measurements done at CERN from April to September, the problem was identified as the combination of two factors:

- the volume resistivity ($\rho_V \sim 100T\Omega cm$ at high voltage $>$ 1kV) of C-lay (Coverlay Kapton foil) was smaller by at least a factor of 100 than expected from datasheets ($\rho_V > 10^4 T\Omega cm$);
- the surface resistivity ($\rho_S \sim 0.1T\Omega/\square$) of the inner Twaron layer (TWi) was also smaller by a factor of 100 compared to expectations, whereas the outer Twaron layer (TWo) was as expected ($\rho_S \sim 10T\Omega/\square$).

The detailed measurements and electrical simulations confirmed that the degraded resistivity and the large surface of the TWi layer created a "conductive" plane just below the Mirror strips, which caused a voltage drop between each strip and TWi: upon HV application (and after early "dielectric" relaxation phase) TWi layer sets at HV/2 voltage (ie intermediate between HV at Cathode and 0V at Anode). A voltage drop is then developed between each strip and TWi: some current is diverted from the voltage divider (being drawn from strips at the Anode side) and flowing across Twi and re-injected into strips at the cathode side. The Coverlay allows current to flow between strips and TWi. Based on the measured resistivity values of the inner Twaron layer (TWi) and the Coverlay, we were able to calculate an excess current that corresponds to the measured $I_{ex}$.

According to the model, there are two negative consequences. Firstly, the amount of current drawn from strips varies depending on their position along the drift direction, leading to uneven voltage degradation and a non-uniform drift electric field that is not parallel to the nominal drift direction. Secondly, a high voltage drop occurs between MSt and TWi across C-lay, potentially exceeding the breakdown level. It is clear that the Field Cage cannot be operated in conditions.

In regards to the issue with the inner Twaron layer (TWi), we have demonstrated that the degraded surface resistivity is specific to that layer (the outer Twaron layer was measured to be okay). We have found that the degraded performance of TWi is due to the use of an Anti-static spray which contains low resistivity components. This spray was applied onto the Coverlay surface just before the TWi layer was laminated. As a result, the TWi resin absorbed the spray components and fixed them on the surface (at the interface with the Coverlay). The use of the anti-static spray was not mentioned in the lamination procedures so that it was not approved by INFN and not explicitly forbidden. Unfortunately, we could not be present at the Company premises for quality controls and checks during FC building process, due to COVID-19 pandemic constraints.

Regarding the Resin type (Resoltech 1054) used in the lamination, we conducted measurements that showed excellent electrical performance ($\rho_V > 10^3 T\Omega cm$ and $\rho_S \sim 10 T\Omega/\square$) when the resin was properly mixed and degassed. By the way we could not exclude that moisture content in the specific resin batch used for laminating TWi could also be a possible cause of electrical performance degradation.

Regarding the Coverlay Kapton foil, we found that Kapton foils with a thickness of $25m$ do not meet the values stated in the datasheet for both dielectric strength and volume resistivity at high voltage. However, we also tested Kapton foils with thicker gauges, which were in good agreement with the datasheet values.

**Adopted solution for High Voltage Issue in Field Cage Production**

In order to address the problem for the next Field Cage (FC1) production, several decisions were made. First, it was decided to forbid using any anti-static spray to keep surfaces clean from dust between consecutive lamination steps (and iso-propyl alchool were the only products allowed for cleaning). Second, the thickness of the Coverlay Kapton was increased from 25 µm to 500 µm (see fig. 7 concerning the new layup). Finally, the same resin (Resoltech 1054) was to be used, but proper mixing and degassing of the resin and hardener were to be ensured.

To ensure quality control, new procedures and checks were implemented. For each batch of resin used during lamination, a sample of resin was prepared to be electrically characterized in terms of volume resistivity ($\rho_V$) and surface resistivity ($\rho_S$). Additionally, for each new laminated layer, measurements of $\rho_V$ and $\rho_S$ were carried out. Volume resistivity $\rho_V$ was measured by taking the mold as the first electrode and a large conductive plate to be stuck to the surface of the layer under test as the second electrode.

The constant presence of the INFN team at the NEXUS Company premises during the entire FC1 production allowed for close monitoring of the building process and quick resolution of new technical issues that arose. Finally, the production schedule was reviewed, optimized, and fixed for the next Field Cages production.

We extend our appreciation to Rui Oliveira from CERN Micro Pattern Technologies Laboratory and to Davide Tommasini, Cedric Urscheler, Sebastien Clement, and Roland Piccin from CERN Polymer Laboratory for their valuable assistance in comprehending and resolving the high voltage issue. We are very grateful for the crucial support we received from INFN and we appreciated the important support from CEA "Antenna" pernonnel at Bld 182.

### 3.1.2 Characterization of FC1

The newly produced Field Cage FC1 was tested for electrical integrity against extraneous currents at the NEXUS Company prior to delivery, and in late February 2023, it was delivered to CERN.

Upon delivery, we proceeded first to extensive surface cleaning and to complete the electrical setup of the cage by selecting and soldering 800 resistors of the two voltage dividers. The values of the individual resistors were measured before and after soldering, and were found to be consistent. Overall, the fluctuations in resistor values had an rms below $3 \times 10^{-4}$ relative. The Cathode was polished and

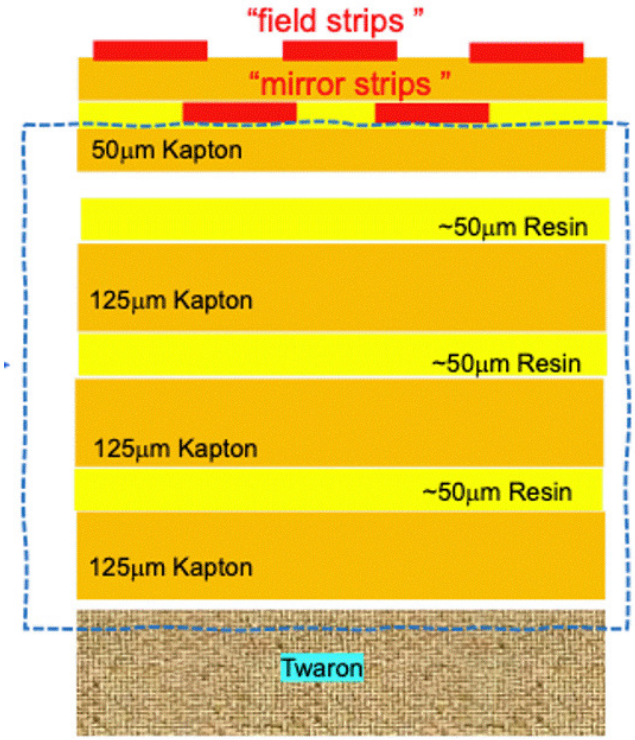


Figure 6: Revised layup in the Field Cage walls

fixed to the cage with the main plane parallel to the first strip plane.

Next, a full 3D metrology (see fig. 7) of FC1 was performed using a laser scan with a resolution of approximately $40\mu m$ per point (see fig. 8). The results of the metrology showed that the geometry of both the cage and cathode met the specifications, with the exception of some degradation in the planarity of the cathode (see fig. 9). However, this degradation does not appear to affect the track resolution. We express our gratitude to Amhed Cherif and colleagues at the Metrology Laboratory in the CERN EN Department for their valuable discussions and support.

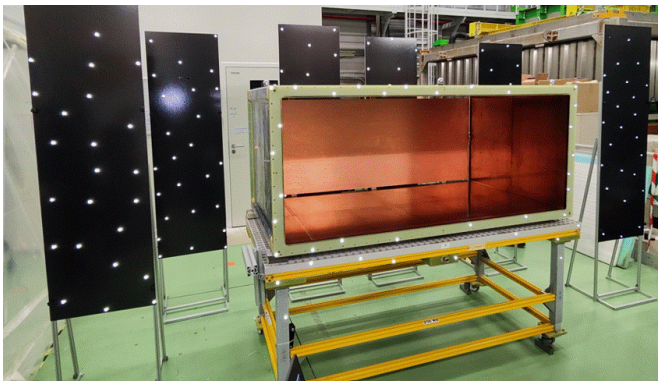

Figure 7: FC1 metrology setup

After sealing FC1 with a special cathode endcap and the anode Module Frame, which was closed with 8 dummy plates, we obtained a gas leak rate of less than $5 \times 10^2 mbarL/s$. This excellent outcome was substantiated by our measurement of Oxygen contamination levels in the few parts per million (ppm) range, which we evaluated by flowing Argon gas after a few volume changes.

After entering FC1 into the Bld.182-2-012 Clean Room, we proceeded to mount eight ERAM modules that had been previously selected and fully tested. Before doing so, we dismounted the dummy plates and cleaned the inner surfaces of the cage using an anti-static roll. In order to reduce the risk

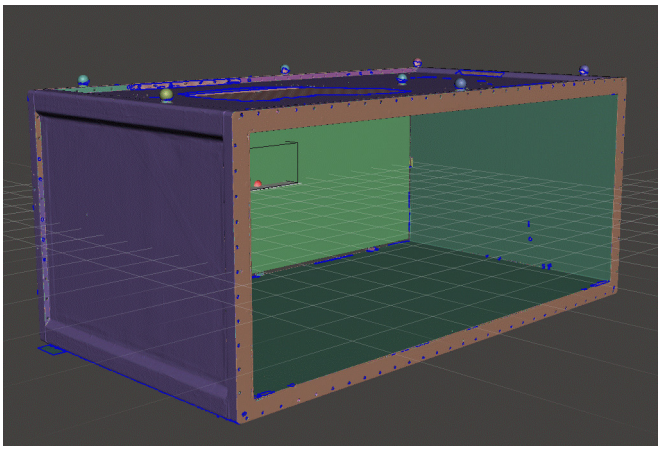

Figure 8: FC1 metrology mesh

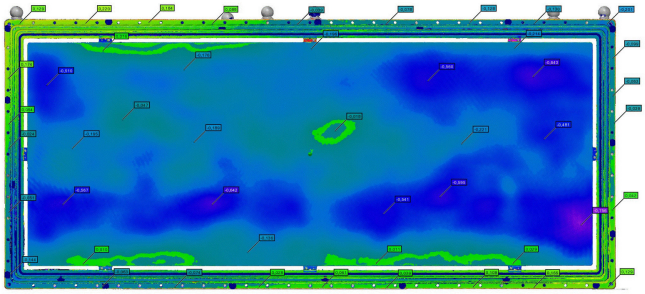

Figure 9: Example of metrology result: FC1 cathode and flange comparison with nominal model

of dust contamination on the inner surfaces, we took special precautions, including the use of a large "grey" room build in front of the Clean room and used as entrance to the Clean room.

Once the modules were mounted, we obtained the first "half" HATPC, which we then moved outside of the Clean Room. We proceeded to flush the HATPC with Argon gas for a week at a rate of $100L/h$ and later with T2K mixture gas. After some volume changes with the T2K gas mixture and increasing the voltage to $-25kV$, we were able to successfully collect Cosmic Rays data. Please refer to our setup in fig.s 11 and 12 and to the first tracks in fig. 13

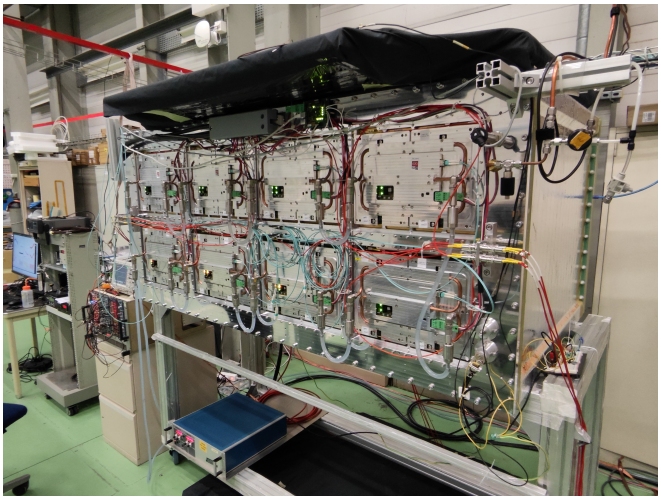

Figure 10: First "half" HATPC equipped with ERAMs at Bld 182

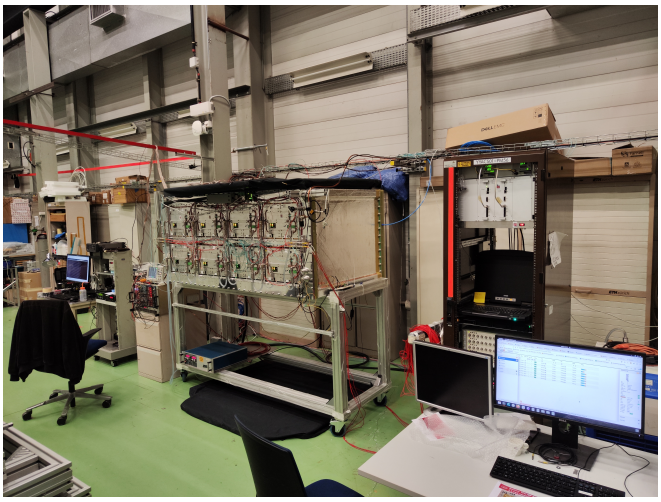

Figure 11: First ”half” HATPC equipped with ERAMs and DAQ setup at Bld 182

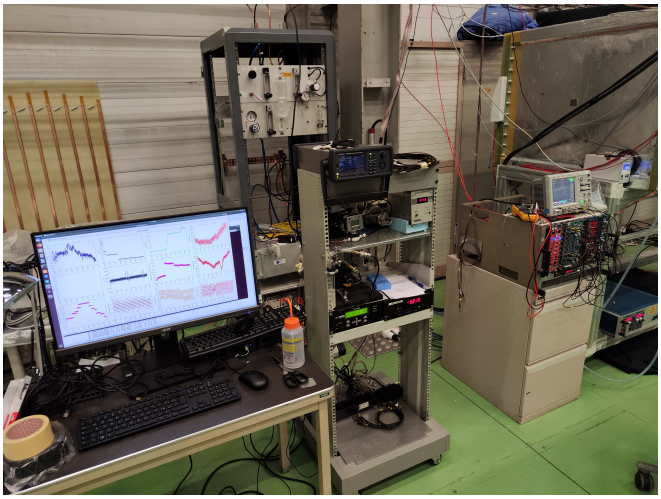

Figure 12: First ”half” HATPC gas system setup at Bld 182

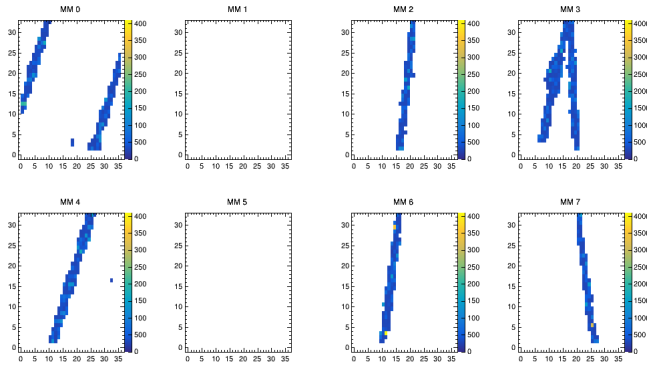


Figure 13: First tracks seen by ”half” HATPC

### 3.1.3 Recovery of first Field Cage FC0, Test Beam in 2024 and full HATPC mechanical assembly tests

The first Field Cage FC0 with corrupted Twaron inner layer is being recovered. First we completely removed the strip layer. Second we completely covered the corrupted Twaron layer with 2mm thick G10 panels in order to keep the Twaron better insulated from the electrodes than was with the 25 microns thick Coverlay. Finally we will glue a new, dedicated strip foil 400 microns thick prepared at the CERN

Micro Pattern Technologies Lab. This final step will be done in early 2024 and as soon as both the new HATPCs will be installed and commissioned at J-Parc.

We are in the process of restoring the first Field Cage FC0, which had corrupted Twaron inner layer. Our first step was to remove the original strip layer completely. We then covered the damaged Twaron layer entirely with 2mm thick G10 panels to provide better insulation between the Twaron and the electrodes than was possible with the original 25-micron Coverlay. In the final step, we will affix a new, specially-designed strip foil that is 400 microns thick, which was produced at the CERN Micro Pattern Technologies Lab. We plan to complete this final step in early 2024, after both new HATPCs are installed and commissioned at J-Parc.

In mid 2024 we plan to have a test beam at the CERN PS facility with FC0 setup as ”half” TPC in order to characterize the Physics performances of an HATPC with low energy particles (100 MeV to 1 GeV).

Currently, the partially recovered FC0 is being utilized as a mechanical mockup to test the assembly of two Field Cages into a complete HATPC and to perform load tests on it. More information can be found in Figures 11 and 12. The load tests conducted on the structure confirmed its exceptional stiffness.

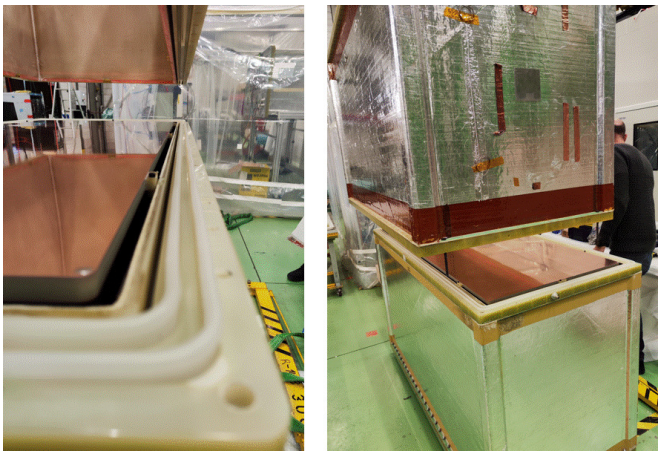

Figure 14: FC0 and FC1 assembled into a ”full” scale HATPC with mechanical parts for lifting and rotation

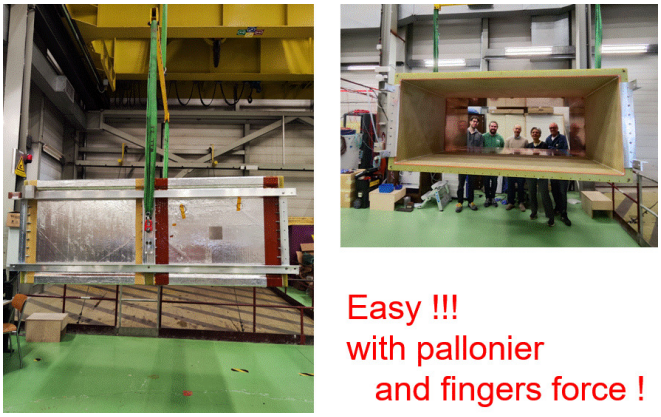


Figure 15: Assembling FC0 and FC1 into a ”full” scale HATPC

### 3.2 Status of the Encapsulated Resistive Anode bulk Micromegas (ERAM) modules

The production of encapsulated resistive anode bulk Micromegas (ERAM) modules is well underway. The produced modules are tested and validated using a X-ray test bench at CERN before their installation in the HA-TPC chambers of the T2K experiment. The X-ray test bench is used to characterize the

detectors by scanning each pad individually and therefore precisely measure the uniformity of the gain and energy resolution over the pad plane. An energy resolution of about 10% was measured.
The first field cage was tested and equipped with eight ERAMs and is under preparation to take cosmics data.

### 3.2.1 Validation of ERAM Performance and Status of Production

The ERAM module consists of a resistive Micromegas detector glued on an aluminium frame on which the readout electronics is fixed directly on its backside. The $42 \times 34$ cm$^2$ detector has 1152 pads of $11.18 \times 10.09$ mm$^2$ disposed in a matrix of 36 pads along $x$ direction and 32 pads along $y$ direction. The pad plane is covered by a resistive layer made of an insulated $50$ $\mu$m Apical polyimide foil (pressed with $150$ $\mu$m glue), on which diamond-like carbon (DLC) is deposited by electron beam sputtering. This resistive layer technology enables to spread the charge over several pads in order to improve the spatial resolution. It can also improve the Micromegas stability and protect the electronics against sparking events. To guarantee a charge dispersion over at least two pads, a DLC surface resistivity $R$ of about 400 k$\Omega/\square$ was chosen.

The production of the ERAMs, at the time of this report writing is well underway, with 23 detectors produced and fully characterized out of the 32 (36 including spares) necessary for the equipment of the two endplates of the two HA-TPCs. A versatile infrastructure has been setup for the quality control: notably two test-benches, one for cosmic rays data-taking and one for test and calibration with X-ray photons from a $^{55}$Fe source. Both are fully instrumented with cooling, readout electronics and DAQ.

The resistive bulk-Micromegas are integrated at CERN/EP-DT-EF and then shipped to building 182 to be glued onto the mechanics and tested. The resistive bulk Micromegas are qualified at different stages of production before a final test during which high voltage is applied over a long period of time to ensure the stability of the detector during future operation. A procedure to validate the performances of the detectors at different stages of production have been perfected to ensure a good operation of the HA-TPCs once installed in Japan.

A dedicated X-ray test bench is used to characterize the detectors by scanning each pad individually and precisely measure the uniformity of the gain and energy resolution over the pad plane. It consists of an aluminium chamber with 3 cm drift distance and a robotic $x - y - z$ arm system on an optical breadboard of $120 \times 60$ cm$^2$ holding a 280 MBq $^{55}$Fe radioactive source. Figure 16 shows a picture of the setup on a table at CERN. A 20 m aluminised mylar window is taped on the chamber side opposite of the ERAM in order to let the X-rays penetrate the gas volume. A mesh cathode allows the electric field to be applied throughout the 3 cm drift volume towards the ERAM grounded mesh. The DLC voltage is set to 350 V. The settings chosen for the AFTER chip are a sampling period of 40 ns and a peaking time of 412 ns. Each step of the robot movement corresponds to a displacement of 0.1 mm, allowing for a precise positioning of the source in the center of each pad of an ERAM. After each installation of a new detector, an alignment procedure is performed in order to ensure the position of the source with respect to the center of each pad. The test bench is fed with the so-called T2K gas mixture (Ar-$CF_4$-i$C_4H_{10}$ $[95\% - 3\% - 2\%]$) with a gas flow of 14 liters/hour. A set of sensors has therefore been added in the gas loop at the exit of the chamber. A Gas Monitoring Chamber identical to the ones deployed at T2K's ND280 detector has been added in the latest ERAM scans. It allows to control the gas conditions in a similar way to what will be performed in ND280.

### 3.2.2 Gain results using X-ray data

To quantify the gain and resolution of each pad, a fit is done over the peak of the reconstructed $^{55}$Fe spectrum. A typical $^{55}$Fe energy spectrum reconstructed is presented in Figure 17. Its associated Gaussian fit for the peak at 5.9 keV is superimposed. The corresponding Argon escape peak is also visible. The ratio between the two peak positions is 1.94. As for the energy resolution, it is defined as: $\frac{\Delta E}{E} = \frac{\sigma}{\mu}$, with $\sigma$ being the Gaussian standard deviation and $\mu$ being the fitted $K_\alpha$ line position.

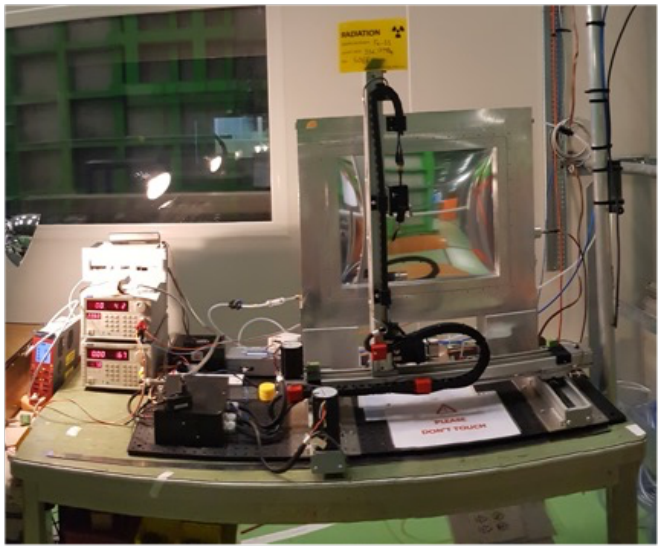

Figure 16: Picture of X-ray test bench at CERN.

Figure 18 depicts the 2D gain maps of eight other ERAMs that have been characterized in a field cage

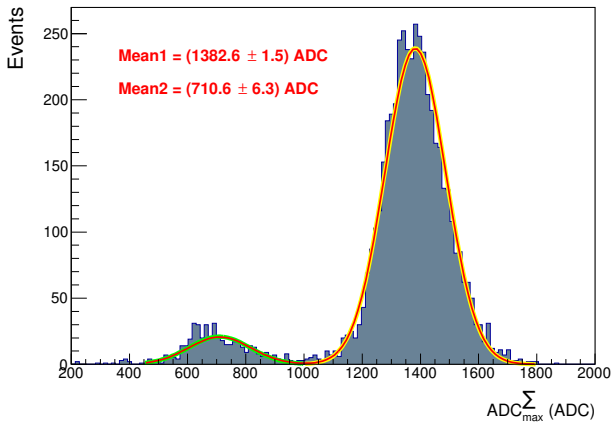


Figure 17: $^{55}$Fe spectrum reproduced from $ADC^{\Sigma}_{max}$ extracted from all the events in one pad.

prototype in testbeam at CERN in November 2022. The map exhibit local non-uniformity between pads whithin a given detector. Figure 19 shows the mean value and local variation in the gain for all analyzed ERAMs. It is found that the absolute gain of the ERAM detectors changes with the design. This effect is still under investigation and is likely due to changes in the production procedures. The mean value of energy resolution is shown in Figure 20 for all analyzed ERAMs. An energy resolution better than 10% is obtained. The 2D gain maps of some ERAM modules have shown grid pattern strangely similar to the shape of the soldermask of the PCB top layer as illustrated by Figure 21.

Indeed, when pressing the DLC on the PCB during the detector assembly, the non-uniformity of the PCB bottom layer results in an unequal distribution of mechanical constraints leading to a reduction of the amplification gap aligned with the stiffener grid. Considering the electric field in the amplification gap, a variation of only few microns is enough to explain the measured gain fluctuations. To solve this problem, the soldermask and copper plates are replaced by a uniform copper mesh. Figure 22 shows the performances of the detector after correction of the PCB bottom layer. The variation in temperature, pressure and humidity was found to have an effect less than 5% on the mean gain. Although a large variations in mean $RC$ and mean gain are observed for the eight tested ERAMS, these differences won't affect the performances as demonstrated by the Test beam papers [13, 5, 6] in which, modules with largely different RC and gains have been tested showing comparable spatial and deposited energy

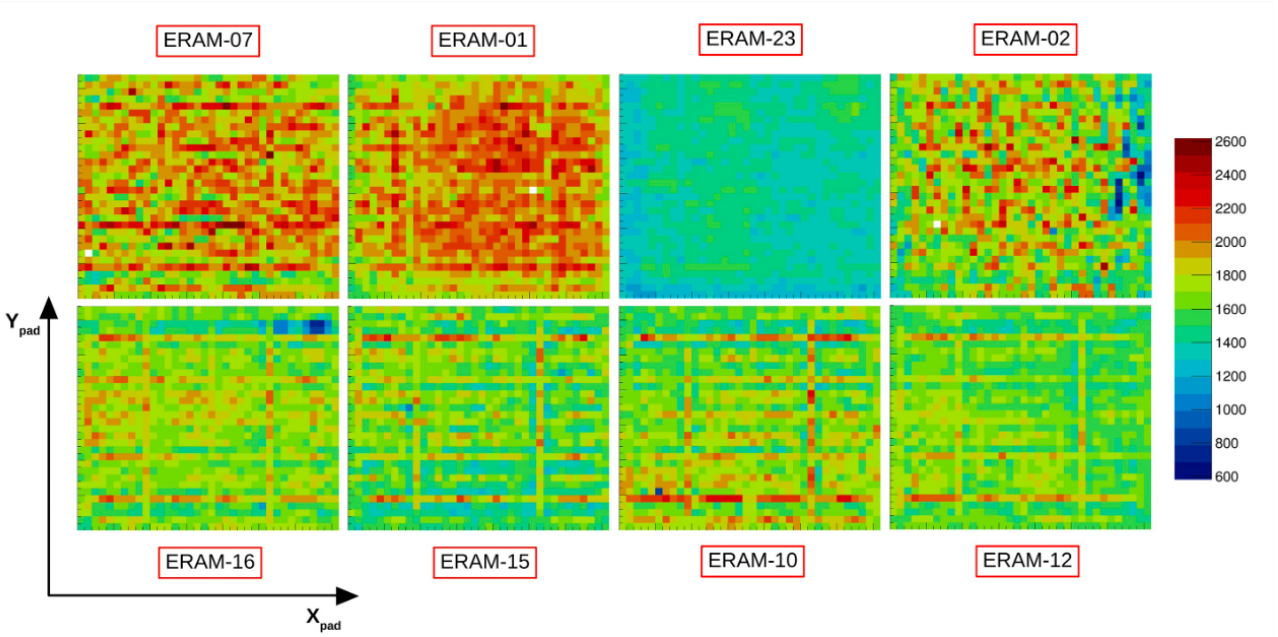


Figure 18: Gain maps of eight ERAMs tested together in a field cage prototype in testbeam at CERN in November 2022.

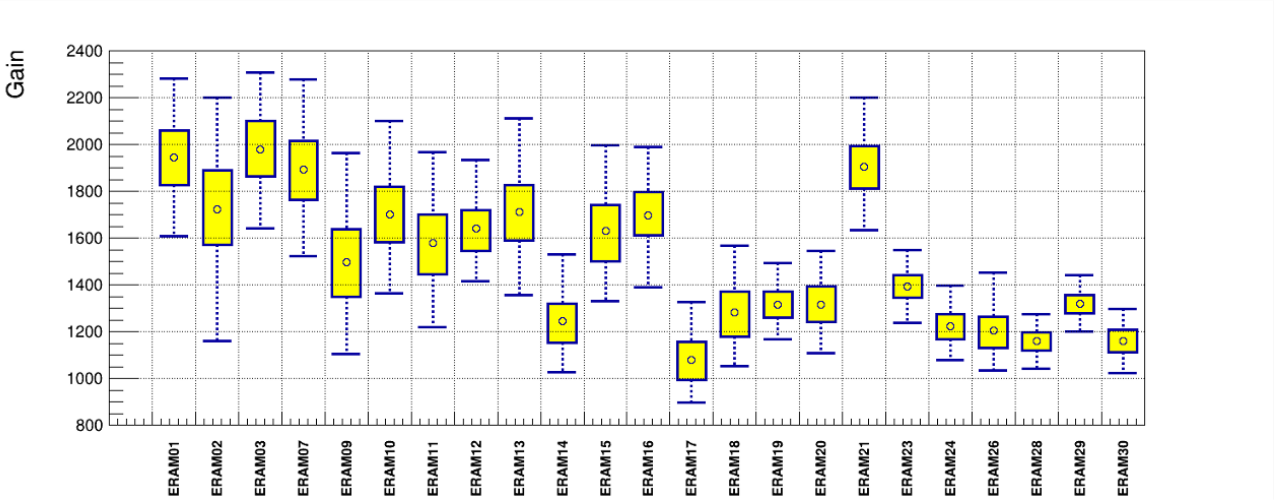


Figure 19: Mean value and local variation in gain for all produced ERAMs. The boxes show the sigma of the distribution for each module while the dotted lines and bars show the extreme values.

resolutions. For what concerns the gain, in fact each pad can be individually calibrated thanks to the careful characterization obtained from the test bench. Concerning the RC, instead, it has been shown in [7] that the resolution change very slowly with RC so non-uniformities in RC do not degrade the resolution.

## 4 The Time Of Flight detector

The Time of Flight (ToF) detector, composed by six modules of 20 scintillator bars each read by arrays of SiPM at each edge, has been commissioned at CERN since September 2022. The detector is designed to provide the particle track direction (inward or outward) to help to reduce the background due to interactions outside the detector fiducial volume. The detector will also be able to provide an cosmic trigger signal which can be used by the other upgrade detectors for calibration purposes. Figure 23 shows a view of the detector at the EHN1 hall during its commissioning. All modules are mounted on

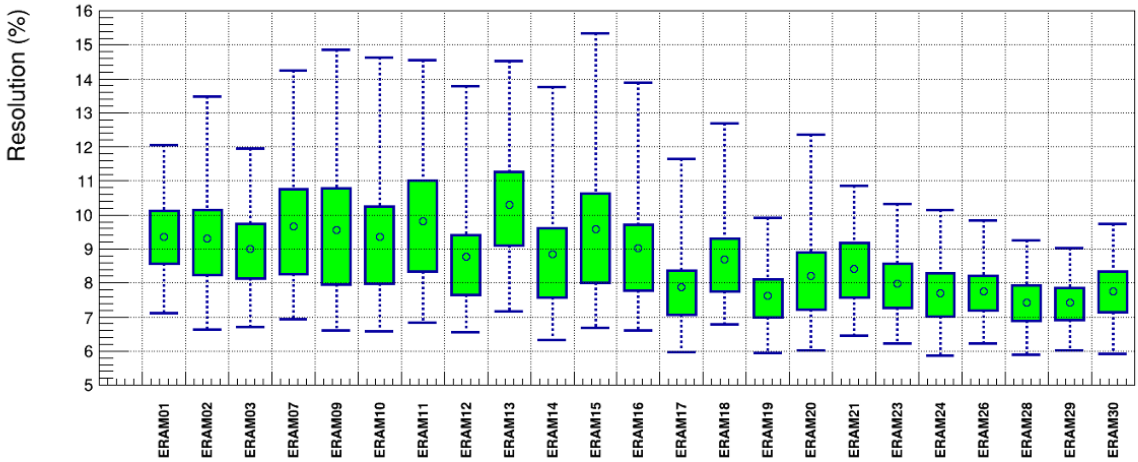


Figure 20: Mean value and local variation in energy resolution for all produced ERAMs. The boxes show the sigma of the distribution for each module while the dotted lines and bars show the extreme values.

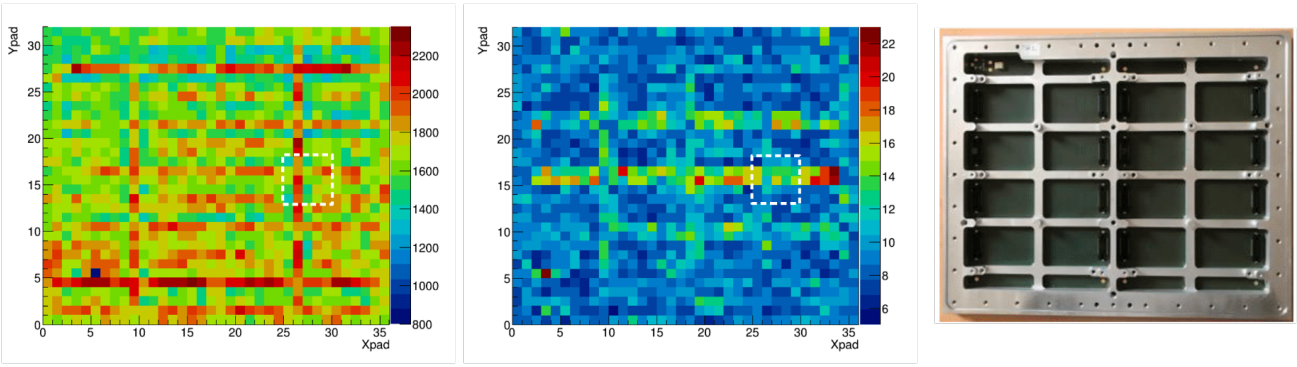


Figure 21: Left: 2D map of the relative gain in ADC of the ERAM-10 module; Middle: 2D map of the energy resolution in % of the ERAM-10 module; Right: PCB top layer: the grey area are 20-35 $\mu$m thick copper + 50 $\mu$m soldermask while the cross hatched area is made of copper mesh only.

the mockup basket (so called "baby basket") and all final elements have been connected : Power supply, Slow Control, Data Aquisition System, final cables.

### 4.1 Hardware status and integration on the overall ND280upgrade project

The detector modules, assembled in the 2020, have been mounted in 2021 on a mock-up of the final ND280 basket which is available at CERN for engineering purposes. Since then the focus have been turned to calibration and commissioning of the electronics, which will ensure the well-functioning and stability of the detector working point and the data-taking, namely the slow control (SC) system and the Data acquisition system (DAQ).

The DAQ system is based on a Waveform and Time to Digital Converter (WTDC) multichannel chip called SAMpler for PICosecond time pick-off (SAMPIC). The system has been fully commissioned since Spring 2022, using both a spare single bar and the full ToF detector. The careful operation of the system with our setup has allowed improve the functionality of the system and cover the acquisition of positive signals with a rather low rate[1]. The operation of the DAQ system with the full detector has also allowed to define the configuration which will be suitable for the data-taking in Japan, as well as to start to define monitoring processes which will allow to identify possible channel failures in almost

[1]The system has been developed mainly to record negative signals with a quite high rate

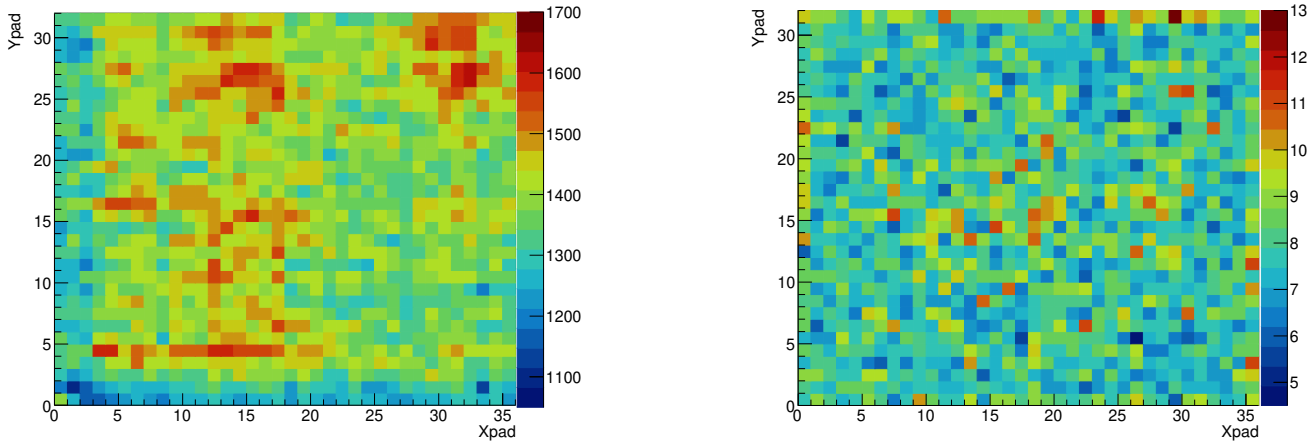


Figure 22: 2D map of the relative gain in ADC (left) and the energy resolution in % (right) after modification of the PCB bottom layer. To be compared with Figure 21.

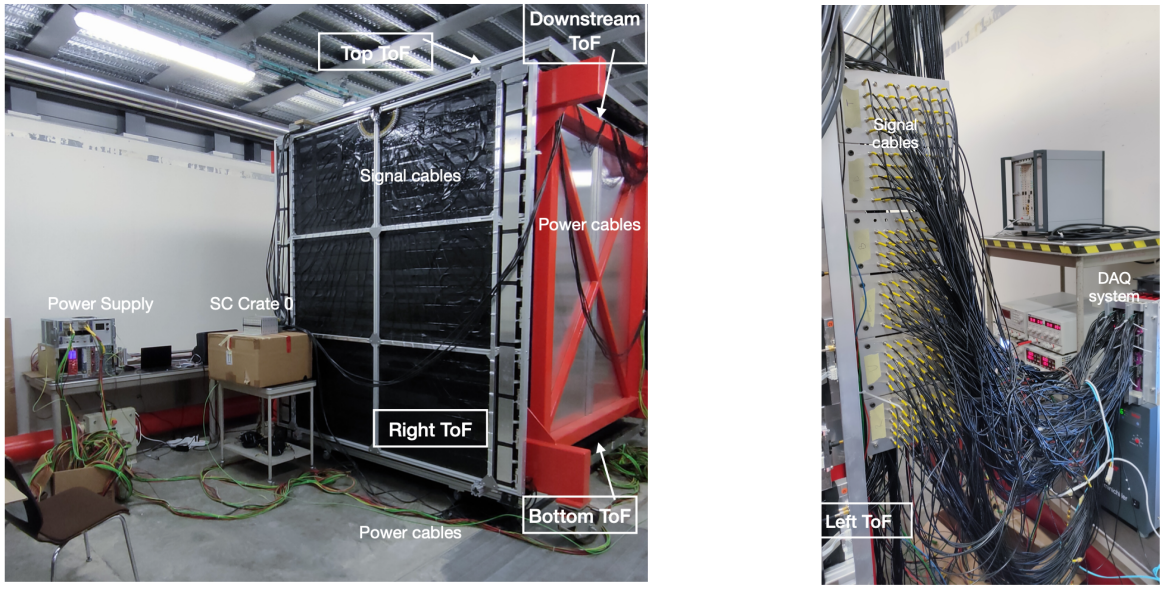


(a) (b)

Figure 23: ToF detector commissioned at CERN with all final elements (power supply, slow control, final cables, DAQ ).

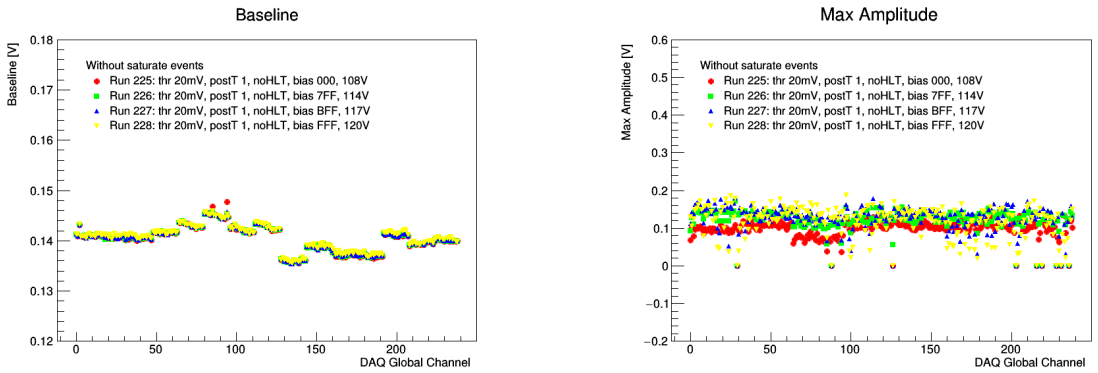


(a) (b)

Figure 24: Summary plots showing the baseline and maximum amplitude for each DAQ channel. The plots are for diagnostic purposes and show an overall good functioning of the detector.

real time. An example of plots which are done regularly for each run are shown in Figure 24. The plots show, on the left, the baseline and, on the right, the maximum amplitude for all the ToF channels (236) for two runs with different bias voltage applied to the SiPM arrays used to read the response of the scintillators. These graphs have purely diagnostic purposes. As expected, the baseline values remain consistent among different runs, while we can appreciate an increase in the maximum signal amplitude as the bias voltage increases. One can notice that in Figure 24b some channels have baseline value equal to 0. These are channels being switched off since noisy or having an identified hardware problem. These issues will be fixed before the detector shipment to Japan.

For the SC system, a careful calibration campaign of the temperature sensors which will monitor the temperature of the electronic boards (PT100 sensors) and of the electronics at the modules edges (NTC sensors) has been performed. After calibration, the response of any sensor is within 1 degree from the reference used for the campaign. Figure 25 shows the temperature of the 20 slow control boards for a run during the TOF commissioning at CERN. The temperature for the two crates are shown with different colors. Temperature variations are observed to be within 1°C.

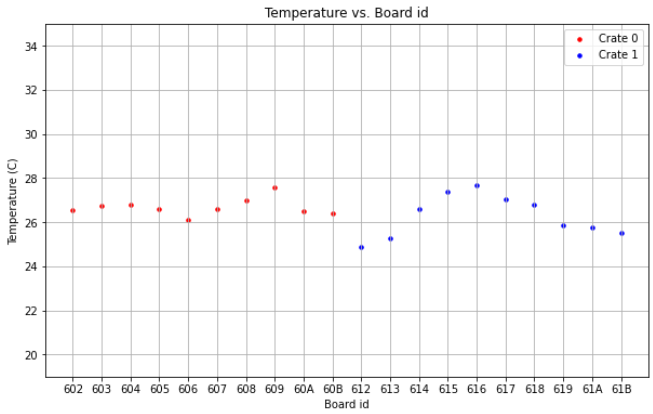


Figure 25: ToF slow control boards temperature for a run during the commissioning at CERN.

## 4.2 ToF schedule

The detector will be unmounted from the Baby Basket, where it's currently installed at CERN, at the beginning of May 2023. The shipment to JPARC is planned for early June. The installation on the ND280 basket is planned by the end of June for the upstream and bottom module, while for the other

modules the installation will be done only after all other upgrade detectors. Before installation, all modules will be tested on surface to verify the well functioning of all photosensors and electronics.

### 4.3 Simulation and Reconstruction Software developments

In the last months, good progress has been done on the software side as well. A first code for the reconstruction has been developed and tested with real data, allowing also to validate the performances of the detector. This is a C++ code written to be easily implemented inside the ND280 software framework, as well as with the MIDAS banks data format. The data coming from the MIDAS Front-End are analysed and converted into ROOT files, that will then be directly read by ROOTAna. This is fundamental to allow the monitoring of the detector during operations.

All the ongoing data analysis is proving to be extremely useful for the development of the simulation of the TOF. The studies on the singlebar, along with the data from the full detector, lead us to develop a simple model for the waveforms coming from the SiPMs arrays. This relatively simple function is being used to generate simulated samples and try to reproduce what is observed from the data, in particular the time resolution.

The new method of the reconstruction rely on the adjustment of a waveform parametrization. The waveform is adjusted to the the function:

$$WF(t) = A_0 e^{-\frac{(t-A_1)^2}{2\sigma^2}} + A_6$$

with

$$\sigma = \begin{cases} A_2(t - A_1) + A_3, & \text{if } t \leq A_1 \\ A_4(t - A_1) + A_5, & \text{otherwise} \end{cases}$$

This empirical formula adjust nicely, see Fig.26, all the waveforms and it provides a natural form to paramewtrise the detector response by interpolating the $A_i$ values and their correlations obtained from the single bar analysis, see an example in Fig.27. The dependencies with the distance to the sensor are smooth functions that can be parametrised and used for the waveform simulation in the Monte Carlo.

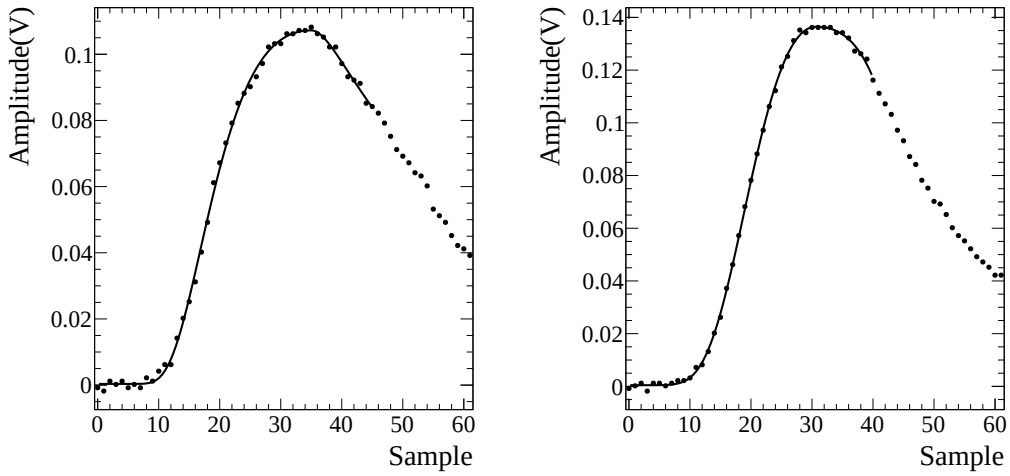


Figure 26: Two Waveforms at different distances to the light sensors adjusted to the modified Gaussian function.

### 4.4 Time resolution estimation with a single bar setup

We have used this reconstruction algorithm to recalculate the time resolution. We define the particle crossing time from the time of the 10% of the adjusted Wave Form. This result, 130 ps at the closest

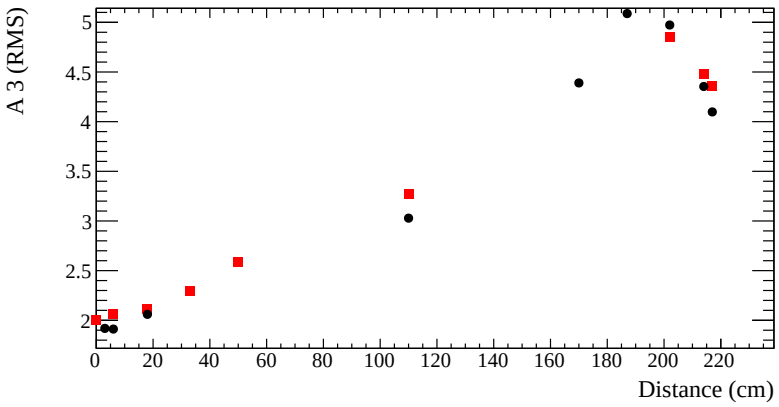


Figure 27: $A_3$ parameter of the WaveForm function as function of the distance to the readout sensor. Black dots represent the result with one bar end and Red squares the resolution from the opposite end.

point to the readout, is compatible with the one used in the past [**empty citation**] and better than the requirements. We can use the time of arrival at both ends of the bar to estimate the position of the entry point of the track in the bar. The obtained values are compatible with the location of the scintillator triggers with a resolution of 2.4 cm for the 2.2 m long bar ($\approx 1\%$). The position can be determined with the ratios of the amplitudes of the signals at both ends, in this case the obtained resolution is 18 cm. The position reconstruction can be used to drive the match of the tracks from the ND280 HA-TPC and sFGD's.

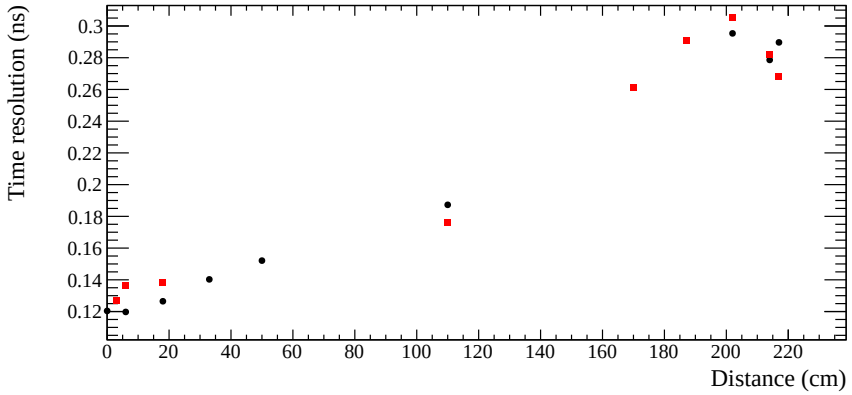


Figure 28: Time resolution as a function of the distance to the readout end obtained with the SAMPIC electronics, the new reconstruction model using the single bar. Results are compatible with the ones obtained with the WaveCatcher and the old recon method. Black dots represent the result with one bar end and Red squares the resolution from the opposite end.

## 5 ND280 Integration

Over the last year, crucial tasks towards the integration, commissioning and operation of the upgraded ND280 were completed or are currently in the final phase. After 3 years without data taking due to the global pandemic situation, the T2K collaboration spend significant efforts in to test all existing components of the ND280 detector and performing maintenance where it was necessary.
This included DAQ tests with all existing detectors, renewal of important network components and upgrading the MIDAS DAQ framework to the latest version.

The pipes and the under-pressure vessel of the electronics cooling system were carefully cleaned. In addition, the existing 12.5 kW chiller was replaced by a 19 kW chiller, powerful enough to also handle the electronics of the upgraded ND280. The whole system was successfully tested and is ready for operation.
The basket modification, necessary to install the new subdetectors, is well advanced. In autumn 2022, first the whole P0D detector was removed and in addition the most upstream TPC, TPC1, of the vertical TPCs. The latter was necessary to have enough space to lift the different P0D modules out of the basket. Afterwards the basket modifications were implemented, cutting the existing diagonal bars and installing new vertical bars on which the SuperFGD and the two HA-TPCs will be fixed. At the different workflow stages, metrology measurements of the basket were performed confirming the FEA results. After the modifications, the most upstream part of the P0D, the usECAL, and TPC1 were reinstalled. DAQ tests with both detectors were successfully performed after the reinstallation.
Also the ND280 magnet, originally used for the UA1 experiment at CERN, underwent significant maintenance procedures. The magnet chiller has been replaced last autumn and also the control software and computing have been upgraded. Preliminary tests were successfully performed. The system will be tested in parallel to the beam operation in the middle of May 2023 to ensure that there is no interference between magnet and beam operation.
The new gas system has been shipped to J-PARC and arrived in Japan the 16th of April 2023. Currently the existing gas system is being removed by a team from INFN Bari and CERN which will be followed by the installation of the new gas system. Including commissioning the system is expected to be ready for use from June 2023 on.
The area in which the new electronics racks will be installed is currently being prepared as also the new cable trays are being installed. This will be completed by end of June 2023 when the first TOF panels will be installed in the basket.
The installation procedure remains unchanged in respect to the one presented last year.

# 6 Project Schedule

Here, we only present the main milestones of the schedule but a detailed Gantt chart can be provided if requested.
The T2K collaboration expects to have neutrino beam in the 2nd half of the Japanese Fiscal Year (JFY) 2023 which began on the 1st of April 2023. The exact time period will be decided in late summer. For the schedule, we assume the 1st of November as the earliest possible date for the beam start. This drives the presented schedule and the collaboration is undertaking all reasonable efforts to have installed by the 1st of November the bottom TPC, the SuperFGD and at least two TOF panels.
The milestones are:

- 03.07.2023: Installation of the bottom and the downstream TOF panel
- 19.07.2023: Arrival of the 1st half the SuperFGD electronics at J-PARC
- 03.08.2023: Arrival of the bottom TPC at J-PARC
- 07.08.2023: Arrival of the 2nd half of the SuperFGD electronics at J-PARC
- 08.2023: Commissioning of the SuperFGD electronics at J-PARC on surface (a pre-commissioning with few FEB cards is already ongoing)
- 18.08.2023: Installation of bottom TPC in the basket
- 01.09.2023: Start installation of the SuperFGD in the basket
- 01.11.2023: Ready for neutrino beam with bTPC, SFGD and two TOF panels (to be confirmed)
- 04.12.2023: Installation of top TPC (if no beam in November)

- 11.12.2023: Completion of ND280 Upgrade installation with installing the last TOF panels in the basket

The commissioning of the fully upgraded ND280 will be an important task in the calendar year 2024.
At this stage of the project, the uncertainties on the schedule are decreasing rapidly, but not completely vanishing. The main uncertainties remaining are related to the production of the SFGD electronics and the shipment of the TPC. To minimize the impact of any possible delay, the schedule is updated and discussed on a bi-weekly basis in the Technical Board, shared with all detector conveners of the existing ND280 and on monthly basis with the whole T2K collaboration. This is supposed to ensure a smooth integration of the new subdetectors in ND280.

While in 2024, the main activity is shifted from CERN to J-PARC, we would like to request to keep the space currently occupied by the TPC group in building 182, at least partly. It would be also necessary to access the clean room punctually in 182. This request is motivated by the fact that field cage 0 (FC0) will be still at CERN and it is foreseen to use it for testbeam measurements in 2024. This would be very useful to understand better the TPC performance we obtain at J-PARC. In addition, in case of problems with the ERAM, we might need to reactivate the X-ray test bench currently installed at building 182.

## References


[1] L. Munteanu et al. "A new method for an improved anti-neutrino energy reconstruction with charged-current interactions in next-generation detectors". In: (2019). arXiv: 1912.01511.

[2] S. Dolan et al. "Sensitivity of the upgraded T2K Near Detector to constrain neutrino and antineutrino interactions with no mesons in the final state by exploiting nucleon-lepton correlations". In: *Phys. Rev. D* 105.3 (2022), p. 032010. arXiv: 2108.11779.

[3] K. Abe et al. "T2K ND280 Upgrade - Technical Design Report". In: (2019). arXiv: 1901.03750.

[4] A. Ershova et al. "Study of final-state interactions of protons in neutrino-nucleus scattering with INCL and NuWro cascade models". In: (Feb. 2022). arXiv: 2202.10402.

[5] D. Attié et al. "Characterization of resistive Micromegas detectors for the upgrade of the T2K Near Detector Time Projection Chambers". In: *Nucl. Instrum. Meth. A* 1025 (2022), p. 166109. arXiv: 2106.12634.

[6] D. Attié et al. "Analysis of test beam data taken with a prototype of TPC with resistive Micromegas for the T2K Near Detector upgrade". In: *Nucl. Instrum. Meth. A* 1052 (2023), p. 168248. arXiv: 2212.06541.

[7] D. Attié et al. "Characterization of Charge Spreading and Gain of Encapsulated Resistive Micromegas Detectors for the Upgrade of the T2K Near Detector Time Projection Chambers". In: (Mar. 2023). arXiv: 2303.04481.

[8] I. Alekseev et al. "SuperFGD prototype time resolution studies". In: *JINST* 18.01 (2023), P01012. arXiv: 2206.10507.

[9] A. Agarwal et al. "Total neutron cross-section measurement on CH with a novel 3D-projection scintillator detector". In: *Phys. Lett. B* 840 (2023), p. 137843. arXiv: 2207.02685.

[10] Saúl Alonso-Monsalve et al. "Artificial intelligence for improved fitting of trajectories of elementary particles in inhomogeneous dense materials immersed in a magnetic field". In: (Nov. 2022). arXiv: 2211.04890.

[11] A. Blondel et al. “A fully active fine grained detector with three readout views”. In: *JINST* 13.02 (2018), P02006. arXiv: 1707.01785.

[12] A. Agarwal et al. “Total neutron cross-section measurement on CH with a novel 3D-projection scintillator detector”. In: *Physics Letters B* 840 (2023), p. 137843.

[13] D. Attié et al. “Performances of a resistive MicroMegas module for the Time Projection Chambers of the T2K Near Detector upgrade”. In: *Nucl. Instrum. Meth.* A957 (2020), p. 163286. arXiv: 1907.07060.